

Scientific paper

Synthesis, Crystal Structure and Biological Activity of Two Triketone-Containing Quinoxalines as HPPD Inhibitors

Xinyu Leng,¹ Chengguo Liu² and Fei Ye^{1,*}¹ Department of Chemistry, College of Arts and Sciences, Northeast Agricultural University, Harbin 150030, China² Department of State Assets Management, Northeast Agricultural University, Harbin 150030, China

* Corresponding author: E-mail: yefei@neau.edu.cn

Tel: +86-451-55190070

Received: 04-03-2022

Abstract

Two new triketone-containing quinoxaline derivatives were designed by fragment splicing strategy and synthesized using 3,4-diaminobenzoic acid and substituted cyclohexanedione as starting materials. Both compounds were characterized by IR, ¹H and ¹³C NMR, HRMS and X-ray diffraction. 3-Hydroxy-5-methyl-2-(quinoxaline-6-carbonyl)cyclohex-2-en-1-one (**6a**) crystallized in the triclinic system, space group *P*₁, *a* = 7.9829(2) Å, *b* = 8.1462(2) Å, *c* = 10.7057(3) Å, α = 84.3590(10)°, β = 89.7760(10)°, γ = 87.4190(10)°, *Z* = 2, *V* = 692.12(3) Å³, *F*(000) = 296, *D*_c = 1.335 Mg/m³, μ (MoK α) = 0.095 mm⁻¹, *R* = 0.0683 and *wR* = 0.1983. 3-Hydroxy-5,5-dimethyl-2-(3-ethoxyquinoxaline-6-carbonyl)cyclohex-2-en-1-one (**6b**) crystallized in the monoclinic system, space group *P*2₁/*c*, *a* = 10.1554(6) Å, *b* = 9.6491(6) Å, *c* = 17.7645(10) Å, β = 90.784(2)°, *Z* = 4, *V* = 1740.59(18) Å³, *F*(000) = 720, *D*_c = 1.299 Mg/m³, μ (MoK α) = 0.092 mm⁻¹, *R* = 0.0462 and *wR* = 0.1235. Physicochemical property comparison and ADMET prediction showed that compound **6a** had similar properties to the commercial herbicide mesotrione. Molecular docking results showed that the interactions between **6a** and AtHPPD were similar to mesotrione. Moreover, the extended aromatic ring system and the additional alkyl form more interactions with the surrounding residues. Examination of AtHPPD inhibition and herbicidal activity showed that **6a** had similar inhibition values to mesotrione and had a superior inhibitory effect on *Echinochloa crus-galli*.

Keywords: Triketone-containing quinoxaline derivatives; Synthesis; Single-crystal structure; Molecular structure information; Herbicidal activity

1. Introduction

Herbicides that inhibit 4-hydroxyphenylpyruvate dioxygenase (EC 1.13.11.27, HPPD) have been used in agriculture for weed control since the 1970s.¹ HPPD is one of the α -keto acid-dependent, non-heme, Fe(II)-dependent enzymes belonging to the 2-His-1-carboxylate facial triad family, and is involved in tyrosine catabolism, which is necessary for most aerobic organisms.^{1–3} *L*-tyrosine is converted to 4-hydroxyphenylpyruvic acid (HPPA) by a transamination catalyzed by tyrosine aminotransferase (TAT). Subsequently, HPPA is converted to homogentisic acid (HGA) by a complex biochemical reaction catalyzed by HPPD. In plants, HGA is converted to plastoquinone and tocopherol,^{4–7} and its absence leads to bleaching symptoms, necrosis, and plant death.^{8,9} Therefore, HPPD is an important enzyme class discovered in recent years that targets herbicides. HPPD inhibitor herbicides are characterized by broad spectrum weed control, flexibility, remarkable plant selectivity, good environmental com-

patibility, low toxicity, and high efficiency.^{9–11} Based on their structure, they can be classified into three categories: Triketones, isoxazoles, and pyrazoles.^{12,13} Triketone derivatives are among the best-studied herbicides and generally contain both triketone and aromatic ring components.^{14,15} Unfortunately, with the widespread use of HPPD herbicides recently, more and more weeds have developed resistance to these active ingredients, which is not limited to the target site.^{16,17} This highlights the importance of developing new HPPD herbicides to effectively manage weed resistance and improve weed control efficiency. Inspired by our previous reports and interest in HPPD herbicides,^{18–22} two novel triketone-containing quinoxaline derivatives were designed and synthesized (Figure 1). Comparisons of physical and chemical properties, ADMET parameters (absorption, distribution, metabolism, excretion, and toxicity), and molecular docking were performed. The biological results showed that compound **6a** had similar inhibition values to the commercial herbicide mesotrione.

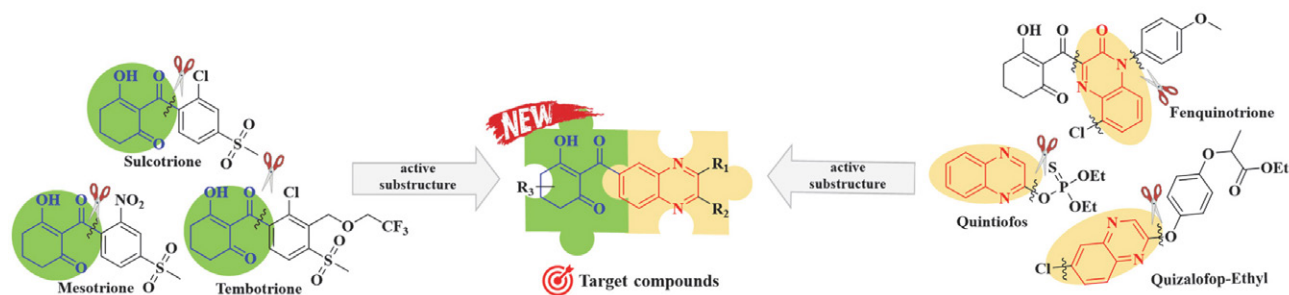


Figure 1. Design of the target compounds.

2. Experimental

2. 1. Materials and Characterization

All reagents were purchased from Shanghai Aladdin Biochemical Technology Co. and were of analytical grade that could be used without any purification. Melting points were measured using a Shanghai INESA melting point instrument (WRS-3) and were uncorrected. The IR spectrum was recorded in KBr pellets using a Bruker ALPHA -T instrument. The NMR spectrum was recorded with a Bruker AV -400 MHz spectrometer (Bruker Company, DEU) using CDCl_3 as solvent and tetramethylsilane (TMS) as internal standard. High-resolution mass spectrometry (HRMS) data were obtained using a Bruker micrOTOF-Q II 10410 spectrometer. X-ray diffraction data were obtained using a RAPID-AUTO area detector diffractometer.

2. 2. Preparation of the Quinoxaline-6-carboxylic acid (2)

In a three-neck flask (100 mL), 3,4-diaminobenzoic acid (10 mmol) was stirred in distilled water, 10% sodium dioctyl sulfosuccinate (SDOSS, 10 mmol) and substituted diketones (**1**, 12 mmol) were added, and the mixture was stirred at room temperature for 4 h.²³ After the reaction, the mixture was filtered under vacuum, the filter cake was dried and recrystallized with EtOH/water to give quinoxaline-6-carboxylic acid (**2**).

2. 3. Preparation of the Acid Chloride (3)

Compound **1** (2 mmol) was dissolved in CH_2Cl_2 (40 mL) in a three-neck flask (100 mL), to which sulfoxide chloride (3 mmol) and DMF (0.1 mL) were added and refluxed for 2 hours.²⁴ Compound **3** was isolated by removing the solvent.

2. 4. Preparation of Enol Ester Compounds (5)

Compound **3** (2.4 mmol) and substituted 1,3-cyclohexanedione (2.1 mmol) were dissolved in CH_2Cl_2 (30 mL), and triethylamine (Et_3N , 2.3 mol) was added dropwise and reacted at 0 °C for 6 h.²⁵ After completion of the

reaction, the mixture was washed three times with aqueous HCl (50 mL, 1 M), followed by washing with saturated sodium chloride solution (50 mL), drying with anhydrous MgSO_4 , and then removing the solvent by filtration under reduced pressure, leaving a solid residue. Compound **5** was obtained by purifying the crude product by silica gel column chromatography (ethyl acetate : petroleum ether = 1:3).

2. 5. Preparation of Triketone-Containing Quinoxalines (6)

The synthetic pathway of **6a** and **6b** is shown in Figure 2. Compound **5** (1 mmol), Et_3N (12 mmol), CH_3CN (13 mmol), and acetone cyanohydrin (AC, 5 mmol) were mixed in CH_2Cl_2 (30 mL) and the reaction was carried out at 25 °C for 6 h.²⁶ After completion of the reaction, the solution was washed three times with aqueous HCl (30 mL, 1 M), followed by washing with saturated aqueous NaCl (30 mL), drying with anhydrous MgSO_4 , and evaporation of the solvent. Compound **6** was obtained by purifying the crude product by silica gel column chromatography (ethyl acetate : petroleum ether = 4:1). Supporting information includes IR, ^1H NMR, ^{13}C NMR, and HRMS information for compounds **6** (Figures S1-S8).

3-Hydroxy-5-methyl-2-(quinoxaline-6-carbonyl)cyclohex-2-en-1-one (6a), Yellow solid; yield: 58%; m.p. 132.5–133.5 °C, IR (KBr, cm^{-1}) 3063–2847 ($-\text{CH}_2-$, $=\text{CH}$), 1651–1608 ($\text{C}=\text{O}$), 1578–1543 ($\text{C}=\text{C}$), ^1H NMR (400 MHz, CDCl_3 , ppm) δ 16.81 (s, 1H, OH), 8.90 (s, 2H, Ar-H), 8.26–7.81 (m, 3H, Ar-H), 2.83 (s, 1H, CH), 2.67–2.29 (m, 4H, $2\times\text{CH}_2$), 1.17 (d, $J = 6.1$ Hz, 3H, CH_3). ^{13}C NMR (100 MHz, CDCl_3 , ppm) δ 197.82, 196.18, 193.95, 146.02, 145.53, 144.16, 142.17, 140.08, 129.59, 129.08, 128.79, 112.95, 26.74, 20.82. HRMS (ESI): calculated for $\text{C}_{16}\text{H}_{14}\text{N}_2\text{O}_3$ $[\text{M}+\text{H}]^+$ 283.1077, found 283.1080.

3-Hydroxy-5,5-dimethyl-2-(3-ethoxyquinoxaline-6-carbonyl)cyclohex-2-en-1-one (6b) Yellow solid; yield: 42%; m.p. 162.7–163.5 °C; IR (KBr, cm^{-1}) ν 3039–2904 ($-\text{CH}_2-$, $=\text{CH}$), 1670–1661 ($\text{C}=\text{O}$), 1550 ($\text{C}=\text{C}$), ^1H NMR (400 MHz, CDCl_3 , ppm) δ 17.01 (s, 1H, OH), 8.49–7.58 (m, 4H, Ar-H), 4.51–4.45 (m, 2H, CH_2), 2.77–2.60 (m, 2H,

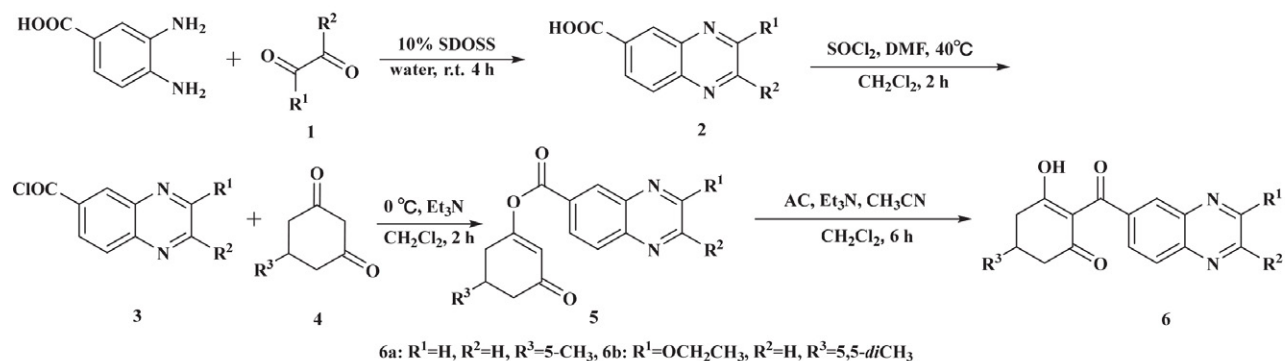


Figure 2. The synthetic route for the compounds 6.

CH₂CO), 2.42 (s, 2H, CH₂), 1.48 (t, *J* = 7.1 Hz, 3H, CH₃), 1.18 (s, 6H, 2×CH₃). ¹³C NMR (100 MHz, CDCl₃, ppm) δ 197.14, 196.11, 194.02, 157.78, 148.05, 146.13, 142.02, 139.80, 129.13, 128.64, 128.42, 112.37, 77.37, 76.74, 74.66, 51.96, 45.97, 31.13, 28.33. HRMS (ESI): calculated for C₁₉H₂₀N₂O₄ [M+H]⁺ 341.1500, found 341.1496.

2. 6. Crystal Structure Determination

Compound **6** was dissolved in EtOAc to form a nearly saturated solution. The crystals grew during the volatilization of the solvent at room temperature in the dark. The crystal was mounted on a RAPID-AUTO area detector diffractometer with MoKα radiation ($\lambda = 0.71073 \text{ \AA}$) at 293(2) K. The crystal structures were solved by direct methods and refined using SHELXS-97 and SHELXL-97.^{27,28} The symmetric equivalent reflectance was used to optimize the shape and size of the crystal. The H atom was then constrained to an ideal geometry with a C-H distance of 0.93–0.98 Å. The $U_{iso}(H)$ value for the methyl H atoms was set to 1.5 $U_{eq}(C)$ and 1.2 $U_{eq}(C)$ for the other H atoms. Crystal packing diagrams were prepared using the xp software. Cambridge Crystallographic Data Center under supplemental publication numbers CCDC 2150405 (**6a**) and 2150406 (**6b**). Copies of the data are available free of charge on request from CCDC, 12 Union Road, Cambridge CB21EZ, UK [www.ccdc.cam.ac.uk/data_request/cif].

2. 7. AtHPPD Inhibitory Experiments in Vitro

Homogentisate 1,2-dioxygenase (HGD) and *Arabidopsis thaliana* HPPD (*AtHPPD*) were prepared and purified according to methods described in the literature.²⁹ Mesotrione, compounds **6**, and *AtHPPD* were preincubated for 25 minutes, then a mixture of appropriate amounts of HGD, HPPA, FeCl₂ (1 mM), ascorbic acid (20 mM), and 4-(2-hydroxyethyl)-1-piperazineethanesulfonic acid (HEPES, 20 mM) buffer (pH 7.0) was added sequentially.^{9,30} An initial screening of the inhibitory effect of each compound was performed at a concentration of 10 μM to determine the final concentration range of the IC₅₀. The

test compounds were dissolved in DMSO and diluted with buffer to various concentrations before use. The IC₅₀ of residual activity was calculated by fitting the curves for different concentrations of the compounds at specific substrate concentrations.

2.8. Herbicidal Activity Assay

All test weeds were purchased from the seed market in Harbin, China. Mesotrione and compounds **6** were tested against the weeds *Echinochloa crus-galli* (EC), *Setaria faberi* (SF), *Digitaria sanguinalis* (DS), Amaranthaceae *Amaranthus retroflexus* (AR), and broadleaf *Abutilon juncea* (AJ) by post-emergence application.¹⁰ Mesotrione and compounds **6** were prepared using DMSO as solvent and Tween 80 (0.1 g/mL) as emulsifier. These solutions were diluted with distilled water to the required concentration and then sprayed on the test plants in the greenhouse. The clay soil was Mollisols-Cryolls clay loam with a pH of 7.3. Approximately 15 weed seeds from EC, SF, DS, AR, and AJ were planted in paper cups, covered with 1.5 cm of soil, and grown in a greenhouse at 18–28 °C and 78% humidity. Broadleaf weeds and monocotyledonous weeds were treated at the two-leaf stage and one-leaf stage, respectively. Once weeds reached the appropriate stage, they were treated with the inhibitors at doses of 0.045 and 0.090 mmol/m² (approximately 150 and 300 g ai/ha). Seeds of the positive control group were treated with the commercial herbicide mesotrione. After 10 days of treatment with these compounds, herbicide activity was measured visually, with each treatment repeated three times.¹²

2. 9. Computational Chemistry

Physical and chemical property comparison, ADMET prediction, and molecular docking were performed using Discovery Studio 2019 (DS, Biovia Inc., CA, USA), and electronegativity was calculated using SYBYL-X 2.0. The 3D structure of mesotrione, compounds **6a** and **6b** was created using Chem3D 15.1, and the molecular structures were further optimized using the MM₂ minimization module. The crystal structure of the protein was down-

loaded from Protein Data Bank (PDB ID: 5YY6, <http://www.rcsb.org/pdb>). 5YY6 was processed before molecular docking, all hydrogen atoms were added, all heteroatoms, ligands and water molecules were removed. Then, the Clean Protein Tool in DS was used to complete incomplete residues, remove excess protein conformations, hydrogenate, and assign the associated charges. The active site was defined using a binding sphere of the native ligand. Molecular docking was performed using the CDOCKER module, and parameters were set to default values. The crystal structure of 5YY6 contained the native ligand 94L, and the ligand molecules at the active site of the complex were abstracted and redocked into the binding pocket. The root mean square deviation (RMSD) was calculated.³

3. Results and Discussion

3.1. Description of the Crystal Structures and Hydrogen Bonding

The crystallographic data and structural refinement details for **6a** and **6b** are given in Table S1. **6a** crystallized in triclinic $P\bar{1}$ -space group with a unit cell volume of 692.12(3) Å³, the cell dimensions are: $a = 7.9829(2)$ Å, $b = 8.1462(2)$ Å, $c = 10.7057(3)$ Å, $\alpha = 84.3590(10)^\circ$, $\beta = 89.7760(10)^\circ$, $\gamma = 87.4190(10)^\circ$, and $Z = 2$. **6b** crystallizes in monoclinic $P2_1/c$ space group with a unit cell volume of 1740.59(18) Å³, the cell dimensions are: $a = 10.1554(6)$ Å, $b = 9.6491(6)$ Å, $c = 17.7645(10)$ Å, $\beta = 90.784(2)^\circ$, and $Z = 4$.

The molecular structures of compounds **6a** and **6b** with the numbering of the atoms are shown in Figure 3. Selected bond lengths and bond angles of **6a** and **6b** are listed in Table S2. The molecule is not coplanar; both crystal structures of compounds **6a** and **6b** consist of two ar-

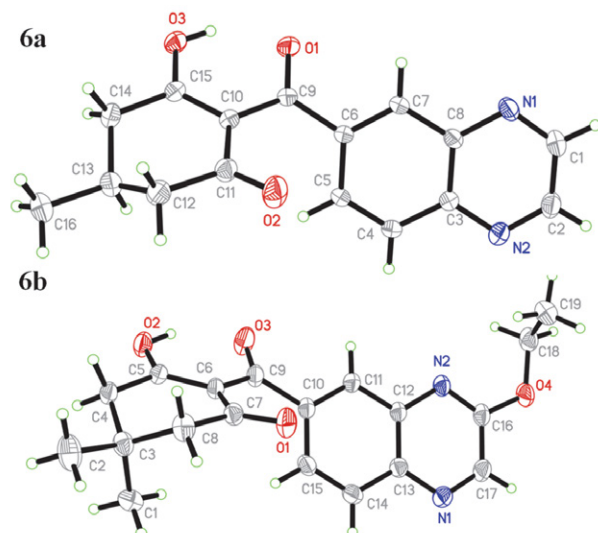


Figure 3. Molecular structures of compounds **6a** and **6b**.

omatic moieties: a cyclohexanedione (A) and a quinoxaline (B). In compound **6a**, for example, the C-C bond length was entirely within the range of the typical C-C bond length (1.54 Å).³⁰ The bond length of C(15)-O(3) was 1.3162(15), which was shorter than the typical C-O length (1.42 Å); the bond length of C(10)=C(15) (1.3841(16) Å) and C(9)-O(1) (1.2490(15) Å) was also longer than the typical C=C length (1.34 Å) and C=O length (1.21 Å).^{31–33} These results suggest a conjugative effect between carbonyl, hydroxyl, and C=C bond. In addition, the C(6)-C(9) bond length (1.4892(16) Å) was shorter than the typical C-C length, which could be due to a π - π conjugation between carbonyl and benzene of quinoxaline. The dihedral angles of part A and part B in compound **6a** and **6b** were 50.32° and 53.80°, respectively. And the cyclohexanedione in both compounds belongs to the half-chair conformation.

The presence of π - π packing interactions, hydrogen bonding, and van der Waals forces resulted in an ordered

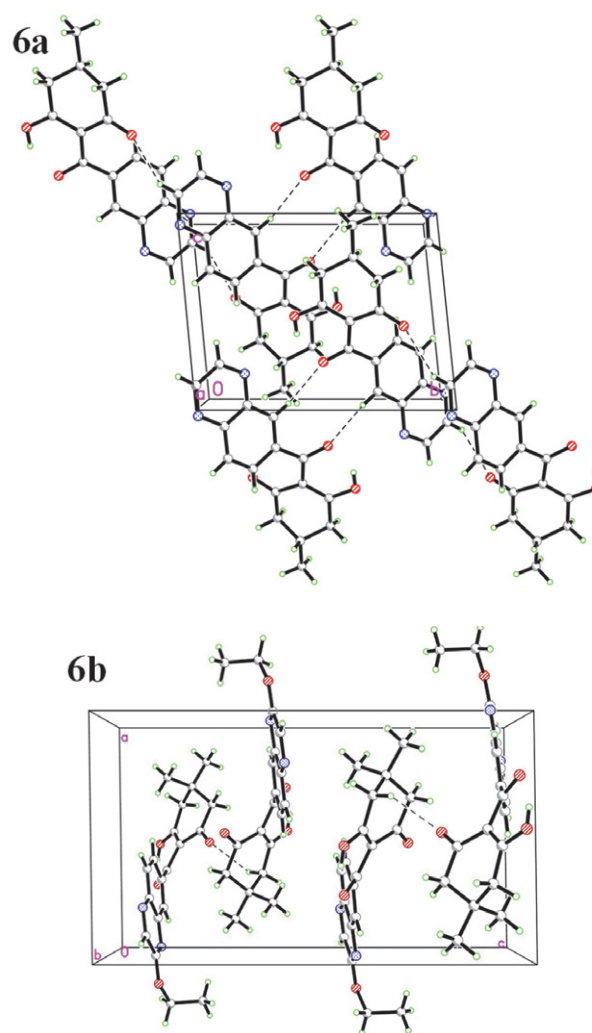
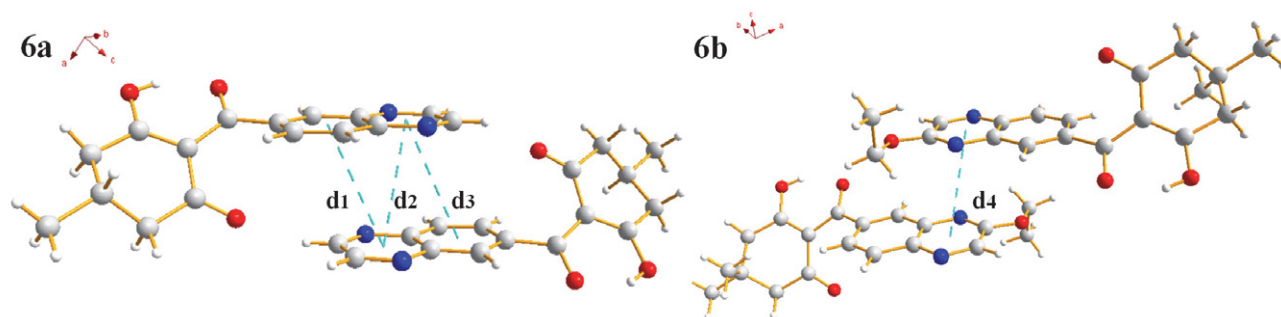


Figure 4. Molecular packing diagram of **6a** and **6b**, hydrogen bonds are shown as dashed lines.

Table 1. Hydrogen bonding parameters in the structures of **6a** and **6b**.

	D-H...A	d(D-H)	d(H...A)	d(D...A)	Symmetry codes	∠DHA
6a	C(7)–H(7)...O(1) ^a	0.9302(11)	2.514(1)	3.2713(15)	1–x, –y, 1–z	138.754(75)
	C(2)–H(2)...O(2) ^b	0.9295(17)	2.4973(13)	3.1763(21)	1–x, –y, –z	130.071(103)
	C(12)–H(12B)...N(2) ^c	0.9699(16)	2.7456(13)	3.5689(20)	1–x, 1–y, –z	143.073(99)
6b	C(4)–H(4B)...O(1) ^d	0.9703(14)	2.5100(11)	3.3190(18)	1–x, –0.5+y, 0.5–z	140.789(86)

**Figure 5.** π - π packing interactions between two molecules.

crystal arrangement with high symmetry and regularity (Figure 4). Compound **6a** formed the packing through the hydrogen bonds C(7)–H(7)...O(1), C(2)–H(2)...O(2), and C(12)–H(12B)...N(2). Compound **6b** formed the packing through hydrogen bonds C(4)–H(4B)...O(1). The hydrogen bonding data are shown in Table 1. As shown in Figure 5, the distance between aromatic rings is within the limited range of typical π - π packing interaction ($d_1 = 3.8537(1)$ Å, $d_2 = 3.6850(1)$ Å, $d_3 = 3.8537(1)$ Å, $d_4 = 3.7647(2)$ Å).

3. 2. Spectroscopic Studies

Compounds **6** were confirmed by IR, ^1H and ^{13}C NMR, and HRMS. Let us take compound **6a** as an example. The IR analysis confirmed the presence of methylene and =CH- group at 3063–2847 cm^{-1} , carbonyl at 1651–1608 cm^{-1} , and C=C bond at 1578–1543 cm^{-1} . The NMR data indicated the possible structure of the compound. The ^1H NMR signals at δ 16.81 ppm are associated with the hydroxyl group of enol. The signals at δ 7.81–8.90 ppm are associated with the five Ar-H of the pyrazine and benzene rings. The signal at δ 2.83 ppm is associated with the hydrogen on the tertiary carbon. The signals at δ 2.37–2.68 ppm and 1.17 ppm are associated with the methylene and methyl groups, respectively. The ^{13}C NMR data at δ 193.95–197.82 ppm show the presence of the carbon atom of enol. The signals at δ 128.79–146.02 ppm relate to the pyrazine and benzene rings and signals at δ 112.95 ppm refer to the carbon between three enols. The signals at δ 20.82–20.74 are characteristic of the remaining saturated carbon atoms. The $[\text{M}+\text{H}]^+$ ion of **6a** was calculated with Chemdraw 15.1 as 283.1007; the actual signal found was 283.1080.

3. 3. AtHPPD Inhibition and Herbicidal Activities

The IC_{50} values against *AtHPPD* in vitro of mesotrione and target compounds **6** are shown in Table 2. The IC_{50} values of mesotrione, **6a**, and **6b** were 0.23, 0.46, and 6.41 μM , respectively. Compound **6a** showed similar inhibition values as mesotrione, possibly because they share the same skeletal structure. The herbicidal effects of mesotrione and compounds **6** against EC, SF, AJ, DS, and AR are listed in Table 2. Weeds treated with compounds **6a** and **6b** showed similar symptoms to mesotrione, suggesting that these target compounds are potential HPPD inhibitors. All compounds tested showed no inhibition in monocotyledonous weeds (AG, DS, and AR). Compound **6a** showed similar inhibitory activity against EC and SF as mesotrione. Notably, **6a** had the superior EC inhibitory activity, suggesting that the scaffold of compounds **6** could be further modified as herbicides.

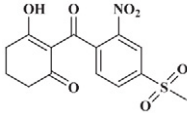
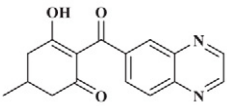
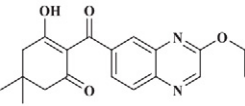
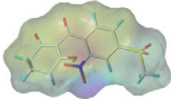
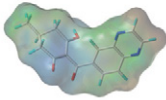
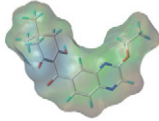
Table 2. Inhibitory activities and post-emergence herbicidal activities (inhibition rating 0–100) of compounds **6a** and **6b** (150 g ai/ha).

compounds	IC_{50} (μM)	Inhibition (%) ^a				
		EC	SF	AJ	DS	AR
Mesotrione	0.23	B	A	G	E	G
6a	0.46	A	B	G	G	G
6b	6.41	F	F	G	G	G

^a Rating scale of inhibition percentage in relation to the untreated control: A, 100%; B, 99–90%; C, 89–70%; D, 69–50%; E, 49–30%; F, 29–20%; G, 0–19%.

The comparisons of physical and chemical properties were studied and are shown in Table 3. Certain sim-

Table 3. Comparison of physical and chemical properties of mesotrione, **6a** and **6b**.

	Mesotrione	6a	6b
Structure			
MW ^a	340.33	282.29	340.37
Log p^a	0.26	1.68	2.78
HBAs ^a	7	5	6
HBDs ^a	2	1	1
RBs ^a	4	2	4
ARs ^a	1	2	2
SA ^a	317.34	280.81	362.96
electronegativity ^b			

ilarities of these compounds at the molecular level were confirmed by the hydrogen bond acceptors (HBAs), hydrogen bond donors (HBDs), rotatable bonds (RBs), aromatic rings (ARs), and electronegativity. When comparing the log p of **6a** and **6b**, it was found that **6a** has a relatively low value that favors herbene transfer and absorption,³⁴ and that compound **6a** has a similar surface area (SA) to mesotrione, which is advantageous for compound **6a** to enter the active pocket. In addition, experiments on *AhH*-PPD inhibition and herbicide activity showed that compound **6a** had a stronger inhibitory effect than compound **6b**. This is likely due to the p - π conjugation between pyrazine and ethoxy, with ethoxy acting as an electron donor and enhancing the inhibitory effect.

3. 4. ADMET Prediction

ADMET prediction has received special attention in drug development. The predicted parameters of mesotrione, **6a** and **6b** are shown in Table 4. Both compounds **6a** and mesotrione were similar in terms of solubility degree, cytochrome P450 2D6 (CYP2D6) prediction, and plasma protein binding ability (PPB). Apparently, compound **6a** was better absorbed than mesotrione. CYP2D6 prediction showed that these two compounds could successfully pass through the first stage of metabolism. The PPB prediction values of the two compounds were not correct, which could lead to low bioavailability because they do not attach to the carrier protein.^{35,36} On the other hand, in the case of compound **6b**, although it has good CYP2D6 prediction and absorption degree, its solubility degree and PPB prediction value are unsatisfactory, leading to a decrease in its activity. In conclusion, compound **6a** has similar pharmacokinetic properties to the commercial herbicide mesotrione, confirming that it has some prospect of weed control.

Table 4. The ADMET prediction of mesotrione, **6a** and **6b**.

	Mesotrione	6a	6b
Solubility Level ^a	4	3	2
Absorption Level ^b	1	0	0
CYP2D6 Prediction ^c	false	false	false
AlogP98 ^d	0.093	1.698	2.776
PPB# prediction ^e	false	false	True

^a Solubility Level: Categorical solubility level. 2: Yes, low.

^b Absorption Level: Absorption Level. 0: Good absorption.

^c CYP2D6: cytochrome P450 2D6. <0.161: false, non-inhibitor; >0.161: true, inhibitor.

^d AlogP98: the logarithm of the partition coefficient between *n*-octanol and water. <4.0: Binding is <90%; >4.0: Binding is >90% and Binding is <95%

^e PPB: Plasma Protein Binding ability. <-2.209: \geq 90%, false; >-2.209: \leq 90%, true.

3. 5. Molecular Docking

Molecular docking was an essential tool for computer-aided drug design (CADD), which correctly predicted

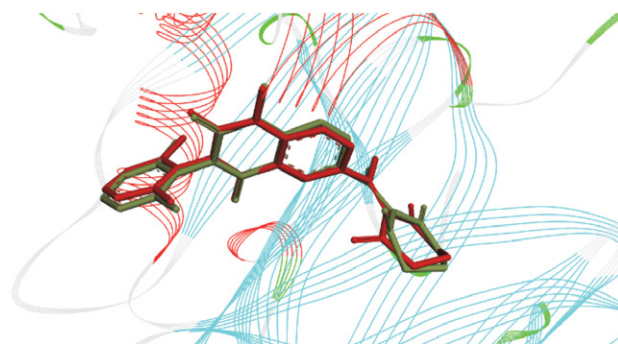


Figure 6. The ligand compared using the CDOCKER docking method (the newly docked ligand was red and the native ligand was green).

the interaction between the inhibitor and herbicide target enzymes.³⁷ To verify the feasibility of molecular docking, the native ligand 94L was redocked to the target protein. The superposition of the conformation of the native ligand with the newly docked conformation is shown in Figure 6. The conformation of the native and redocked ligand 94L was almost completely overlapping with an RMSD value of 0.5549 Å (< 2 Å), confirming the accuracy of the CDOCKER docking procedure.³

The mesotrione, **6a** and **6b** were selected for the molecular docking experiments to predict the binding pattern with 5YY6. Compounds **6a** and **6b** hardly differed from mesotrione in terms of geometric complementarity of the binding position in the active pocket. Mesotrione and **6a** occupied the active pocket almost completely, whereas **6b** occupied only part of the pocket (Figure S9 in the Supporting Information). The enol structure and carbonyl groups in these compounds all coordinate with Co²⁺. In compound **6a**, the distances between the Co²⁺ and O atoms were 2.02 Å and 1.86 Å, respectively, similar to mesotrione. The benzene moiety of compound **6a** formed a π - π -stacked interaction with PHE424, similar to that of mesotrione, and HIS226 formed a new interaction with the O atom, further improving the binding ability of the ligand. The additional interactions of compound **6a** with PRO280 and VAL269 resulted in strong binding to the receptor, which may explain the similarity of the AtHPPD inhibitory activity of compound **6a** with mesotrione.

4. Conclusion

In summary, two new triketone-containing quinoxaline derivatives were developed and synthesized as novel HPPD herbicides. Both compounds exhibited certain HPPD inhibitory activities. In particular, compound **6a** showed similar AtHPPD inhibition and herbicidal activity to the commercial herbicide mesotrione, as demonstrated by physical and chemical property comparisons, ADMET prediction, and molecular docking study.

Acknowledgements

This work was supported by the National Nature Science Foundation of China (grant number 22077014) and the Under-graduate SIPT Program of Northeast Agricultural University (grant number 202110224014).

Supporting information includes the crystallographic data and structure refinement details for compounds **6** (Table S1), selected bond lengths and bond angles for crystals of compounds **6** (Table S2), the IR, ¹H, ¹³C NMR and HRMS spectra of compounds **6** (Figures S1-S8), the receptor-ligand interaction, and coordination patterns of mesotrione and compounds **6** with AtHPPD (Figure S9).

5. References

- E. Rocaboy-Faquet, L. Barthelmebs, C. Calas-Blanchard, T. Nogueir, *Talanta*, **2016**, *146*, 510–516. DOI:10.1016/j.talanta.2015.09.030
- L. Serre, A. Sailland, D. Sy, P. Boudec, A. Rolland, E. Pebay-Peyroula, C. Cohen-Addad, *Structure*, **1999**, *8*, 977–988. DOI:10.1016/S0969-2126(99)80124-5
- Y. Fu, S. Q. Zhang, Y. X. Liu, J. Y. Wang, S. Gao, L. X. Zhao, F. Ye, *Ind. Crops Prod.*, **2019**, *137*, 566–575. DOI:10.1016/j.indcrop.2019.05.070
- S. O. Duke, *Pest Manag. Sci.*, **2012**, *68*, 505–512. DOI:10.1002/ps.2333
- K. Lei, X. W. Hua, Y. Y. Tao, Y. Liu, N. Liu, Y. Ma, Y. H. Li, X. H. Xu, C. H. Kong, *Bioorg. Med. Chem.*, **2016**, *24*, 92–103. DOI:10.1016/j.bmc.2015.11.032
- R. Beaudegnies, A. J. F. Edmunds, T. E. M. Fraser, R. G. Hall, T. R. Hawkes, G. Mitchell, J. Schaezter, S. Wendeborn, J. Wibley, *Bioorg. Med. Chem.*, **2009**, *17*, 4134–4152. DOI:10.1016/j.bmc.2009.03.015
- P. S. Garcia, A. L. D. Moreau, J. C. M. Ierich, A. C. A. Vig, A. M. Higa, G. S. Oliveira, F. C. Abdalla, M. Hausen, F. L. Leite, *IEEE Sens. J.*, **2015**, *15*, 2106–2113. DOI:10.1109/JSEN.2014.2371773
- L. X. Zhao, J. F. Peng, F. Y. Liu, Y. L. Zou, S. Gao, Y. Fu, F. Ye, *J. Agric. Food Chem.*, **2022**, *70*, 1003–1018. DOI: 10.1021/acs.jafc.1c05210 DOI:10.1021/acs.jafc.1c05210
- F. Ndikuryayo, B. Moosavi, W. C. Yang, G. F. Yang, *J. Agric. Food Chem.*, **2017**, *65*, 8523–8537. DOI:10.1021/acs.jafc.7b03851
- D. W. Wang, H. Y. Lin, R. J. Cao, T. Chen, F. X. Wu, G. F. Hao, Q. Chen, W. C. Yang, G. F. Yang, *J. Agric. Food Chem.*, **2015**, *63*, 5587–5596. DOI:10.1021/acs.jafc.5b01530
- Y. Fu, M. Wang, L. X. Zhao, S. Q. Zhang, Y. X. Liu, Y. Y. Guo, D. Zhang, S. Gao, F. Ye, *Pest. Biochem. Physiol.*, **2021**, *174*, 104811. DOI:10.1016/j.pestbp.2021.104811
- Y. Fu, D. Zhang, S. Q. Zhang, Y. X. Liu, Y. Y. Guo, M. X. Wang, S. Gao, L. X. Zhao, F. Ye, *J. Agric. Food Chem.*, **2019**, *67*, 11839–11847. DOI:10.1021/acs.jafc.9b01412
- H. Huang, M. M. Wang, L. Shu, Y. L. Yan, J. Q. Zhang, J. M. Liu, X. H. Zhan, D. Y. Zhang, *Pest Manag. Sci.*, **2020**, *76*, 4112–4122. DOI:10.1002/ps.5967
- A. Santucci, G. Bernardini, D. Braconi, E. Petricci, F. Manetti, *J. Med. Chem.*, **2017**, *60*, 4101–4125. DOI:10.1021/acs.jmedchem.6b01395
- M. Baalouch, A. D. Mesmaeker, R. Beaudegnies, *Tetrahedron Lett.*, **2013**, *54*, 557–561. DOI:10.1016/j.tetlet.2012.11.081
- N. E. Hausman, S. Singh, P. J. Tranel, D. E. Riechers, S. S. Kaundun, N. D. Polge, D. A. Thomas, A. G. Hager, *Pest Manag. Sci.*, **2011**, *67*, 258–261. DOI:10.1002/ps.2100
- P. M. McMullan, J. M. Green, *Weed Technol.*, **2011**, *25*, 514–518. DOI:10.1614/WT-D-10-00150.1
- W. Hu, S. Gao, L. X. Zhao, K. L. Guo, J. Y. Wang, Y. C. Gao, Y. Fu, F. Ye, *Pest Manag. Sci.*, **2022**, *78*, 938–946. DOI:10.1002/ps.6703
- H. M. Song, L. X. Zhao, S. Q. Zhang, T. Ye, Y. Fu, F. Ye, *J. Agric.*

- Food Chem.*, **2021**, *69*, 12621–12633. DOI:10.1021/acs.jafc.1c04621
20. L. Jia, S. Gao, Y. Y. Zhang, L. X. Zhao, Y. Fu, F. Ye, *J. Agric. Food Chem.*, **2021**, *69*, 8366–8379. DOI:10.1021/acs.jafc.1c02221
21. Z. W. Wang, L. X. Zhao, P. Ma, T. Ye, Y. Fu, F. Ye, *Pest Manag. Sci.*, **2021**, *77*, 1724–1738. DOI:10.1002/ps.6193
22. L. Jia, X. Y. Jin, L. X. Zhao, Y. Fu, F. Ye, *J. Agric. Food Chem.*, **2022**, *70*, 5499–5515. DOI:10.1021/acs.jafc.2c01565
23. L. Cuesta, I. Maluenda, T. Soler, R. Navarro, E. P. Urriolabeitia, *Inorg. Chem.*, **2011**, *50*, 37–45. DOI:10.1021/ic101946n
24. F. Ye, Y. Zhai, T. Kang, S. L. Wu, J. J. Li, S. Gao, Y. Fu, *Pest. Biochem. Physiol.*, **2019**, *157*, 60–68. DOI:10.1016/j.pestbp.2019.03.003
25. B. He, J. Dong, H. Y. Lin, M. Y. Wang, X. K. Li, B. F. Zheng, Q. Chen, G. F. Hao, W. C. Yang, G. F. Yang, *J. Agric. Food Chem.*, **2019**, *67*, 10844–10852. DOI:10.1021/acs.jafc.9b04917
26. D. W. Wang, H. Y. Lin, R. J. Cao, Z. Z. Ming, T. Chen, G. F. Hao, W. C. Yang, G. F. Yang, *Pest Manag. Sci.*, **2015**, *71*, 1122–1132. DOI:10.1002/ps.3894
27. G. M. Sheldrick, SHELXS-97, Program for X-ray Crystal Structure Solution. University of Göttingen, Göttingen, Germany, **1997**.
28. G. M. Sheldrick, SHELXL-97, Program for X-ray Crystal Structure Refinement. University of Göttingen, Göttingen, Germany, **1997**.
29. H. Huang, J. Q. Zhang, J. M. Liu, M. M. Wang, L. Shu, Y. L. Yan, X. H. Zhang, P. Wang, X. T. Huan, D. Y. Zhang, *Pest Manag. Sci.*, **2020**, *77*, 1409–1421. DOI:10.1002/ps.6159
30. F. B. Rudolph, B. B. Baugher, R. B. Beissner, *Methods Enzymol.*, **1979**, *63*, 22–42. DOI:10.1016/0076-6879(79)63004-5
31. T. Topal, *Acta Chim. Slov.*, **2021**, *68*, 88–101. DOI:10.17344/acsi.2020.6183
32. Z. H. Yang, X. Li, H. K. Ma, J. Y. Zheng, X. C. Zhen, X. H. Zhang, *Bioorg. Med. Chem.*, **2014**, *24*, 152–155. DOI:10.1016/j.bmcl.2013.11.051
33. M. Y. Huang, W. Xu, J. J. Huang, Y. J. Huang, M. Yuan, *Chinese J. Struct. Chem.*, **2015**, *34*, 497–502. DOI:10.4028/www.scientific.net/KEM.671.497
34. M. A. Ezeokonkwo, O. N. Ogbonna, S. N. Okafor, E. U. Godwin-Nwakwasi, F. N. Ibeanu, U. C. Okoro, *Front. Chem.*, **2017**, *5*, 107. DOI:10.3389/fchem.2017.00107
35. Z. W. Wang, L. X. Zhao, S. Gao, X. Y. Leng, Y. Yu, Y. Fu, F. Ye, *Pest. Biochem. Physiol.*, **2021**, *179*, 104958. DOI:10.1016/j.pestbp.2021.104958
36. L. Jia, L. X. Zhao, F. Sun, J. Y. Wang, X. Y. Leng, S. Gao, Y. Fu, F. Ye, *Pest. Biochem. Physiol.*, **2022**, *187*, 105185. DOI:10.1016/j.pestbp.2022.105185
37. S. Sakkiah, S. Thangapandian, S. John, Y. J. Kwon, K. W. Lee, *Eur. J. Med. Chem.*, **2010**, *45*, 2132–2140. DOI:10.1016/j.ejmech.2010.01.016

Povzetek

V prispevku je opisana priprava dveh novih triketonskih kinoksalinskih derivatov, ki vsebujeta triketone, s strategijo spajanja posameznih fragmentov, sintetiziranih iz 3,4-diaminobenzojske kisline in substituiranega cikloheksandiona kot izhodnih molekul. Oba kinoksalinska derivata so okarakterizirali z IR, ^1H in ^{13}C NMR, HRMS in rentgensko difrakcijo. 3-Hidroksi-5-metil-2-(kinoksalin-6-karbonil)cikloheks-2-en-1-on (**6a**) kristalizira v triklnskem kristalnem sistemu, v prostorski skupini $P\bar{1}$, $a = 7.9829(2)$ Å, $b = 8.1462(2)$ Å, $c = 10.7057(3)$ Å, $\alpha = 84.3590(10)^\circ$, $\beta = 89.7760(10)^\circ$, $\gamma = 87.4190(10)^\circ$, $Z = 2$, $V = 692.12(3)$ Å³, $F(000) = 296$, $D_c = 1.335$ Mg/m³, $\mu(\text{MoK}\alpha) = 0.095$ mm⁻¹, $R = 0.0683$ and $wR = 0.1983$. 3-Hydroxy-5,5-dimethyl-2-(3-ethoxyquinoxaline-6-carbonyl)cyclohex-2-en-1-one (**6b**) crystallized in the monoclinic system, space group $P2_1/c$, $a = 10.1554(6)$ Å, $b = 9.6491(6)$ Å, $c = 17.7645(10)$ Å, $\beta = 90.784(2)^\circ$, $Z = 4$, $V = 1740.59(18)$ Å³, $F(000) = 720$, $D_c = 1.299$ Mg/m³, $\mu(\text{MoK}\alpha) = 0.092$ mm⁻¹, $R = 0.0462$ and $wR = 0.1235$. Primerjava fizikalno-kemijskih lastnosti in ADMET napovedi so pokazale, da ima spojina **6a** podobne lastnosti kot komercialni herbicid mezotriol. Rezultati molekulskega modeliranja so pokazali, da so interakcije med **6a** in AtHPPD podobne tistim pri mezotriolu. Poleg tega razširjeni aromatski obročni sistem in dodatne alkilne skupine povečajo interakcije z okolico. Raziskave inhibicije AtHPPD in herbicidnega delovanja so pokazale, da ima kinoksalin **6a** podobne vrednosti inhibicije kot mezotriol in boljši inhibični učinek na *Echinochloa crus-galli*.



Except when otherwise noted, articles in this journal are published under the terms and conditions of the Creative Commons Attribution 4.0 International License